Systems/Circuits

Infra-Slow EEG Fluctuations Are Correlated with Resting-State Network Dynamics in fMRI

Tuija Hiltunen,[1] Jussi Kantola[1] Ahmed Abou Elseoud,[1] Pasi Lepola,[2] Kalervo Suominen,[2] Tuomo Starck,[1] Juha Nikkinen,[1] Jukka Remes,[1,2] Osmo Tervonen,[1] Satu Palva,[3] Vesa Kiviniemi,[1]* and J. Matias Palva[3]*

Departments of [1]Diagnostic Radiology, and [2]Clinical Neurophysiology, Oulu University Hospital, 90029 OYS, Oulu, Finland, and [3]Neuroscience Center, University of Helsinki, FI-00014 Helsinki, Finland

Ongoing neuronal activity in the CNS waxes and wanes continuously across widespread spatial and temporal scales. In the human brain, these spontaneous fluctuations are salient in blood oxygenation level-dependent (BOLD) signals and correlated within specific brain systems or "intrinsic-connectivity networks." In electrophysiological recordings, both the amplitude dynamics of fast (1–100 Hz) oscillations and the scalp potentials per se exhibit fluctuations in the same infra-slow (0.01–0.1 Hz) frequency range where the BOLD fluctuations are conspicuous. While several lines of evidence show that the BOLD fluctuations are correlated with fast-amplitude dynamics, it has remained unclear whether the infra-slow scalp potential fluctuations in full-band electroencephalography (fbEEG) are related to the resting-state BOLD signals. We used concurrent fbEEG and functional magnetic resonance imaging (fMRI) recordings to address the relationship of infra-slow fluctuations (ISFs) in scalp potentials and BOLD signals. We show here that independent components of fbEEG recordings are selectively correlated with subsets of cortical BOLD signals in specific task-positive and task-negative, fMRI-defined resting-state networks. This brain system-specific association indicates that infra-slow scalp potentials are directly associated with the endogenous fluctuations in neuronal activity levels. fbEEG thus yields a noninvasive, high-temporal resolution window into the dynamics of intrinsic connectivity networks. These results support the view that the slow potentials reflect changes in cortical excitability and shed light on neuronal substrates underlying both electrophysiological and behavioral ISFs.

Introduction

Spontaneous slow fluctuations (0.1–1 Hz) and infra-slow fluctuations (ISFs; 0.01–0.1 Hz) are ubiquitous in brain dynamics. In electrophysiological recordings, these fluctuations have been observed both in single-unit and multiunit firing rates (Werner and Mountcastle, 1963; Albrecht and Gabriel, 1994; Ruskin et al., 1999, 2003; Allers et al., 2002), as well as in amplitude envelopes of fast (>1 Hz) activities in microelectrode field potentials (Leopold et al., 2003), electrocorticography (ECoG) (Monto et al., 2007; Ko et al., 2011), magnetoencephalography, and electroencephalography (EEG) (Linkenkaer-Hansen et al., 2001). Several studies show that firing-rate fluctuations are strongly correlated with the amplitude envelope fluctuations in distinct brain systems (Allers et al., 2002; Hughes et al., 2011), which suggests a mechanistic relationship between these phenomena. Direct current (DC)-coupled or "full-band" EEG (fbEEG) approaches have shown that the cortical potentials (Aladjalova, 1957; Norton and Jewett, 1965) and scalp potentials (Aladjalova, 1964; Trimmel et al., 1990; Marshall et al., 1998; Vanhatalo et al., 2004; Monto et al., 2008) exhibit ISFs. These slow potential fluctuations are tightly correlated with amplitude envelope fluctuations of faster activities (Aladjalova, 1957; Vanhatalo et al., 2004; Monto et al., 2008).

A large body of fMRI data also shows that blood oxygenation level-dependent (BOLD) ISFs are correlated or anti-correlated among specific constellations of cortical regions, termed resting-state networks (RSNs) or intrinsic-connectivity networks, characterized by a dynamic small world-like network architecture for large-scale brain activity (Biswal et al., 1995; Lowe et al., 1998; Damoiseaux et al., 2006; De Luca et al., 2006). Similar to the infra-slow potential fluctuations, BOLD signals correlate with the amplitude envelopes of concurrently acquired EEG oscillations (Leopold et al., 2003; Goldman et al., 2002; Mantini et al., 2007; Sadaghiani et al., 2010). This suggests that spontaneous EEG potential and BOLD ISFs could be correlated and reflect the same underlying neuronal dynamics. However, so far only indirect evidence supports this hypothesis.

First, active task performance for tens of seconds evokes in parallel a negative potential shift and a positive shift in BOLD response in concurrent recordings (Leistner et al., 2007, 2010). Second, spontaneous ~0.1–0.5 Hz fluctuations in ECoG recordings have a spatial correlation pattern that is similar to BOLD signals (He et al., 2008). Third, event-related slow potentials are topologically and phenomenologically similar to BOLD re-

Received Jan. 18, 2013; revised Oct. 17, 2013; accepted Oct. 27, 2013.

Author contributions: K.S. and V.K. designed research; T.H., A.A.E., P.L., K.S., and V.K. performed research; T.H., J.K., A.A.E., P.L., K.S., T.S., J.N., J.R., S.P., V.K., and J.M.P. contributed unpublished reagents/analytic tools; T.H., J.K., K.S., T.S., J.N., J.R., O.T., V.K., and J.M.P. analyzed data; T.H., J.K., A.A.E., T.S., O.T., S.P., V.K., and J.M.P. wrote the paper.

*V.K. and J.M.P. contributed equally to this work.

The authors declare no competing financial interests.

This research was supported by Academy of Finland Grants 111711, 123772, 253130, and 256472; Strategic Centre for Science, Technology and Innovation SalWe Grant WP 302; and the Finnish Medical Foundation.

Correspondence should be addressed to Vesa Kiviniemi, Department of Diagnostic Radiology, Oulu University Hospital, P.O. Box 50, Oulu 90029 OYS, Finland. E-mail: Vesa.Kiviniemi@oulu.fi.

DOI:10.1523/JNEUROSCI.0276-13.2014

 0270-6474/14/340356-07$15.00/0

sponses in several cognitive tasks (Khader et al., 2008). Finally, ISFs in a subset of scalp EEG contacts share phenomenological similarities, such as task reactivity and association with attention-deficit/hyperactivity disorder symptoms (Helps et al., 2010), with the BOLD ISFs in the default-mode network (DMN) and may be source localized to DMN structures (Broyd et al., 2011). Nevertheless, the issue of whether the spontaneous BOLD fluctuations are directly correlated with concurrent endogenous infra-slow scalp potentials under task-free conditions has remained unresolved.

In the present study, we used concurrent fbEEG and fMRI recordings to address this missing link. We found that independent components of spontaneous infra-slow fbEEG fluctuations were selectively correlated with fMRI–BOLD signals in specific RSNs. These data suggest that scalp potential ISFs and BOLD resting-state dynamics are reflections of the same underlying neurophysiological phenomenon.

Materials and Methods

Subjects. Twenty-one healthy, nonsmoker volunteers (mean age, 24.1 ± 2.8 years; 7 females) participated in the study, which was approved by the Ethics Committee of Oulu University Hospital. Written informed consent has been obtained from each subject individually, in accordance with the Helsinki declaration. All participants (mild-to-moderate caffeine consumers, based on self-reports of consumption of coffee, tea, and soft drinks) were instructed to abstain from caffeine intake since the night before the study (15–18 h). Each simultaneous resting-state fbEEG and fMRI recording lasted 8 min and 30 s.

fbEEG recordings. The electroencephalogram was recorded using Ag/AgCl electrodes placed according to the international 10–20 system with a 32-channel MR-compatible BrainAmp system (Brain Products). Two additional channels were used to record electrocardiogram and electrooculogram. The impedance of each electrode was <10 kΩ, which was obtained by scraping the epithelium of the skin. The EEG data-sampling rate was 5000 Hz on-line, and the bandpass was from DC to 250 Hz. The quality of the fbEEG signal was tested outside the magnet room by an experienced physicist (P.L. or K.S.). The subjects were transferred to the magnet room and carefully placed in the 8-channnel head coil with careful padding to maximize the stability and comfort. They were instructed to simply lay still inside the scanner with their eyes closed, think of nothing particular, and not to fall asleep. The BrainAmp SyncBox was used to ensure that the fbEEG amplifier and the scanner are in synchrony via a transistor–transistor logic pulse.

FMRI acquisition. The functional data were collected on a GE Signa 1.5 tesla whole-body system with an eight-channel receive coil, with an EPI gradient echo sequence (TR, 1800 ms; TE, 40 ms; 280 time points; 28 oblique axial slices; slice thickness, 4 mm; interslice space, 0.4; covering the whole brain; FOV, 25.6 × 25.6 cm, with 64 × 64 matrix; and flip angle, 90°). T1-weighted scans were imaged using 3D fast spoiled gradient echo (FSPGR) BRAVO sequence (TR, 12.1 ms; TE, 5.2 ms; slice thickness, 1.0 mm; FOV, 24.0 cm; matrix 256 × 256; and flip angle, 20°) to obtain anatomical images for coregistration of the fMRI data to standard space coordinates. Physiological signals (heart rate and respiratory volume) were recorded using the scanner's built-in photoplethysmograph placed on a finger of the right hand, and respiratory belt.

fbEEG data preprocessing. fbEEG recordings were processed off-line using the Brain Vision Analyzer (version 2.0, Brain Products). Gradient artifacts due to static and dynamic magnetic field during MRI data acquisition were removed using the average artifact subtraction (AAS) method (Allen et al., 2000). The ballistocardiographic (BCG) artifacts were removed with the same AAS method (Allen et al., 1998). At this point, an experienced physicist (K.S.) verified that there were neither gradient nor BCG artifacts left in the data.

FMRI data preprocessing. Head motion in the fMRI data was corrected using multiresolution rigid-body coregistration of volumes, as implemented in FSL 3.3 MCFLIRT software (Jenkinson et al., 2002). The default settings used were as follows: middle volume as reference; a three-stage search (8 mm rough + 4 mm, initialized with 8 mm results + 4 mm fine grain, initialized with the previous 4 mm step results) with final trilinear interpolation of voxel values, and normalized spatial correlation as the optimization cost function. Brain extraction was performed for motion-corrected BOLD volumes with optimization of the deforming smooth surface model, as implemented in FSL 3.3 BET software (Smith, 2002) using threshold parameters $f = 0.5$ and $g = 0$; and for 3D FSPGR volumes, using parameters $f = 0.25$ and $g = 0$. After brain extraction, the BOLD volumes were spatially smoothed with the fslmaths tool, 5 mm FWHM Gaussian kernel.

fbEEG independent components analysis and spectral analysis. fbEEG data were exported to MATLAB (MathWorks) where the independent components analysis (ICA) was calculated with EEGLAB (version 9.0.0.2b; Delorme and Makeig, 2004) using the Infomax algorithm (Bell and Sejnowski, 1995), which is recommended in EEGLAB tutorial with sub-Gaussian sources detection. The maximum number of components (32) was used, and the resulting components were downsampled to match the fMRI sampling frequency 0.55 Hz (1/1.8 s) by getting an average value of each of the 1.8 s periods. fbEEG independent components (ICs) were characterized by a $1/f$ power spectra that had (mean ± SEM) Hurst exponents of 0.269 ± 0.026 and 0.265 ± 0.020, respectively, for ICs corresponding and not corresponding to BOLD RSNs (see below; difference not significant at $p > 0.9$, t test). The spectra did not reveal conspicuous frequency-dependent differences between RSN and non-RSN ICs.

BOLD RSN definition. For BOLD data, we calculated group probabilistic ICA (PICA) as implemented in MELODIC (Beckmann and Smith, 2004). The same number of components, 32, was used as in the fbEEG ICA decomposition. First, artifact components (e.g., CSF and blood pulsation) motion and white matter were removed. Secondary PICA was performed on the artifact-removed BOLD group data using the same model order of 32, and the resulting components were thresholded (BOLD_ICcleaned) using the same histogram mixture modeling as in fbEEG-fMRI maps to obtain the same threshold level in both measurements. From the BOLD_ICcleaned, eight well known and robustly detectable RSN components (Damoiseaux et al., 2006; Seeley et al., 2007) were selected (BOLD_RSNthresh) and binarized with fslmaths tool (BOLD_RSNbin). The IC definition was based on the expertise of one of the authors (V.K.). The selected networks were visual lateral (VIS LAT), default mode in posterior cingulate cortex (DMNpcc), dorsal attention (DAN), default mode in ventromedial prefrontal cortex (DMNvmpf), salience (SAL), secondary somatosensory cortex (S2), primary motor cortex (M1), and executive (EXEC; see Fig. 2). A list of regions in which BOLD signal correlated with the respective EEG IC is presented in Table 1.

fbEEG ICs and BOLD correlation. Correlation maps between fbEEG IC time series and preprocessed BOLD data were calculated with FSL (version 4.1.4) FEAT by using fbEEG ICs as regressors (fbEEG-fMRI maps). Hemodynamic convolution (gamma function with default settings) was included. After that, the correlation maps were thresholded using histogram mixture modeling as implemented in MELODIC (fbEEG-fMRIthresh maps). The histogram mixture modeling enables unique thresholding for each fbEEG-fMRI map based on inferences from two additional gamma functions in addition to Gaussian modeling. Gaussian–gamma mixture modeling was used because the intensity distribution of the independent components was non-Gaussian, and, hence, simple thresholding based on z-scores cannot accurately control the false-positive rate. In mixture modeling, noise is modeled with the Gaussian, and positive and negative neuronal activity with the two gamma functions is used to model the tails of the distribution. The probability density functions of these models are then evaluated under the alternative hypothesis, and a posterior probability of activation is obtained. A posterior probability of 0.5 is used for symmetrical control over the false-positives and false-negatives (Beckmann and Smith, 2004). The fbEEG–fMRIthresh maps were then binarized using the fslmaths tool in FSL (fbEEG–fMRIbin maps).

To identify within each subject the fbEEG IC that was best correlated with each BOLD_RSNthresh, we calculated spatial correlation coefficients between all fbEEG–fMRIbin maps and each of the selected eight

Table 1. Peak coordinates and cluster sizes of regions where the BOLD signal was correlated with the respective EEG IC

EEG IC	*x*	*y*	*z*	Area	Maximum *t* score	$N_{Voxels} \pm SD$	$N_{Overlap} \pm SD$ Real	$N_{Overlap} \pm SD$ RAND	fslcc ± SD Real	fslcc ± SD RAND	*t* test *p* value
VIS Lat	56	10	40	V2	2.46	20,671 ± 10,676	4668 ± 2983	1416 ± 1048	0.19 ± 0.10	0.06 ± 0.01	2.26E−05
	28	16	38	V2							
DAN	64	22	58	LOC	1.98	17,762 ± 10,027	5175 ± 3037	1008 ± 895	0.19 ± 0.09	0.08 ± 0.02	8.58E−07
	66	73	63	MFG							
DMNvmpf	46	97	47	FP	1.92	18,345 ± 11,462	4276 ± 2344	1268 ± 924	0.17 ± 0.11	0.07 ± 0.02	8.50E−04
Sal	40	64	73	PreMot	2.01	23,555 ± 10,945	4863 ± 2223	1148 ± 888	0.16 ± 0.07	0.08 ± 0.02	2.26E−04
	72	70	34	IFG							
S2	12	49	48	S2 / PO	1.95	21,770 ± 11,884	4774 ± 2653	1119 ± 845	0.15 ± 0.08	0.08 ± 0.01	8.89E−07
	16	70	36	Broca							
	78	47	53	SMG							
M1	44	50	68	M1	2.12	22,141 ± 11,958	3768 ± 2649	1190 ± 825	0.16 ± 0.11	0.07 ± 0.01	1.27E−07
EXEC	62	92	46	FP	1.94	18,768 ± 10,860	2646 ± 1714	1435 ± 954	0.14 ± 0.08	0.06 ± 0.01	1.93E−05
	28	84	52	FP							
	44	80	50	CinG							
DMNpcc	44	30	50	PreCun	2.16	18,853 ± 10,443	4180 ± 2207	1348 ± 972	0.18 ± 0.12	0.07 ± 0.01	1.59E−05
	68	24	49	LOC							
	22	28	49	LOC							

Peak coordinates [Montreal Neurological Institution (MNI)] are reported for cluster components in descending volume order for at least 90% of cumulative volume. CinG, Cingulate gyrus (anterior division); FP, frontal pole; IFG, inferior frontal gyrus (pars opercularis); LOC, lateral occipital (superior division); MFG, middle frontal gyrus; PO, parietal operculum; PreCun, precuneus; PreMot, premotor; SMG, supramarginal gyrus (posterior division); V2, visual area V2 (prestriate cortex); Broca, Broca's area. $N_{Overlap}$, mean number of overlapping voxels; N_{Voxels}, mean number of voxels. The fslcc correlation coefficients indicate the spatial correlation between EEC-IC and BOLD-ICA components for both real and RAND. *p* values (using *t* test) for the comparison of real and randomized overlap voxel counts are reported in the right-most column.

BOLD_RSNbin maps with the FSL fslcc tool. For each of the eight BOLD_RSNbin maps, the fbEEG–fMRIbin map with the greatest correlation coefficient was selected for further analysis. We used the FSL randomization test (randomize version 2.1) to evaluate voxel-by-voxel statistical significance in fbEEG–fMRI correlation maps. For controlling multiple comparisons, we used familywise error correction (FWE) at $p < 0.05$. For each BOLD_RSNbin map and the corresponding best-correlated fbEEG–fMRIbin map, the correlation coefficients with different BOLD_RSNbin maps were averaged among subjects (see Fig. 3). In Figure 3, to test whether these differences between correlation coefficients were significantly different, we also estimated an exploratory (without correction for multiple comparisons) pairwise assessment of each network against each other network. The spatial patterns of EEG IC versus BOLD voxel correlations were significantly different at a level of $p < 0.05$ for all network pairs except DMNvmpf-EXEC, DMNpcc-EXEC, and SAL-S2 (see Fig. 3, small colored circles).

To control that the observed correlations did not arise from random effects or from the selection procedure, we randomized all fbEEG–fMRIbin maps with Matlab and calculated the correlation coefficients with one RSN (DMNpcc) again. We chose DMNpcc because it is thought to be the most active network at rest (Fox et al., 2005; Raichle et al., 2001). The selection and averaging procedure was then applied in a manner identical to that described above. We also calculated the average correlation coefficients between randomized data and BOLD_RSNbin maps [see Fig. 3, white "RAND" (randomized data)].

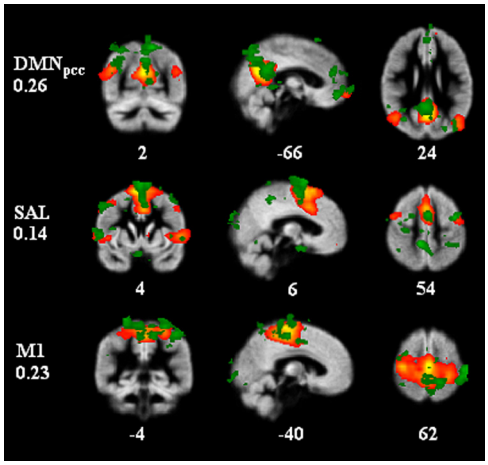

Figure 1. In individual subjects, fbEEG IC time series are correlated with BOLD signals at the voxel level in patterns closely matching those of BOLD ICs. An example of one subject's BOLD_RSNbin (red-yellow) and corresponding best correlation coefficient giving fbEEG–fMRIbin (green) maps. Correlation coefficients between fbEEG–fMRIbin maps and BOLD_RSNbin maps were for DMNpcc 0.26, for SAL 0.14 and for M1 0.23. Numbers at the bottom of the images refer to MNI coordinates (*x*, *y*, *z*).

Results

To investigate the hypothesized relationship between infra-slow scalp potential and BOLD signal fluctuations, we acquired concurrent resting-state fbEEG-fMRI recordings with 21 healthy subjects. After removing MRI and physiological artifacts from fbEEG data (see Materials and Methods), we decomposed the spontaneous fbEEG signals into ICs with ICA. This approach alleviates the volume conduction-caused problem of signal mixing in scalp potential recordings and yields temporally maximally independent signals that are comparable with those defining the RSNs in fMRI. We then quantified the correlation between the fbEEG–IC time series decimated to the fMRI sampling rate and voxel level–BOLD signal time series. We found that at the individual subject level, a large number of significant EEG–BOLD correlations were observed (Fig. 1, green regions). Intriguingly, these patterns appeared similar to those of the RSNs found with ICA of fMRI data in numerous studies. To quantify this similarity, we mapped the RSNs in the present data by probabilistic ICA of the fMRI recordings (Fig. 1, red-yellow regions) and evaluated the spatial correlation between binarized maps of fbEEG IC versus BOLD voxel correlations and those of BOLD ICs (Fig. 1, correlation coefficients). Comparisons of the best-correlated maps showed that even at the single-subject level, the fbEEG-IC versus BOLD-voxel correlation maps were indeed highly colocalized with well known RSNs, reflected in BOLD ICs (Fig. 1).

To test systematically whether this phenomenon was robust across subjects, we selected eight BOLD ICs that corresponded to the following RSNs: VIS LAT, DMNpcc, DAN, DMNvmpf, SAL, S2, M1, and EXEC (Fig. 2, red-yellow regions). For each of these, we identified the map of statistically significant correlations between fbEEG ICs and BOLD voxels that had the greatest spatial correlation with the BOLD IC map and averaged them across subjects by taking the voxel-by-voxel mean of selected correlation maps with AFNI 3dMean tool (Fig. 2, green regions). These

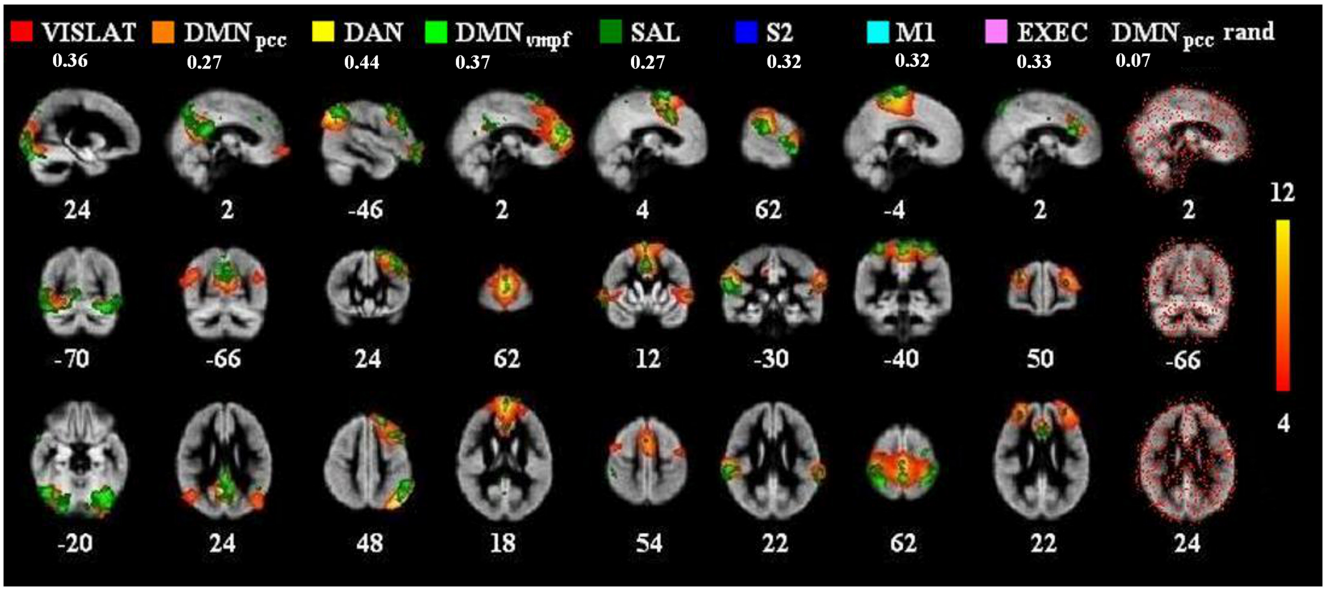

Figure 2. Group-level resting-state fbEEG ICs and fMRI BOLD signals exhibit correlations in the same anatomical regions than fMRI ICs. Eight selected BOLD_RSNthresh maps (red-yellow, *z*-score thresholding in right color bar) from group PICA, and corresponding thresholded and FWE-corrected fbEEG-fMRI maps (green). The rightmost map is a randomized fbEEG-fMRIbin map for BOLD DMNpcc (thresholded 0.1–1). Numbers below RSN names present correlation coefficients (fslcc) between these BOLD_RSNthresh maps and fbEEG–fMRI maps. Numbers at the bottom of the images refer to MNI coordinates (*x*, *y*, *z*). The first eight maps are organized in descending order of grand average correlation coefficients (as in Fig. 3).

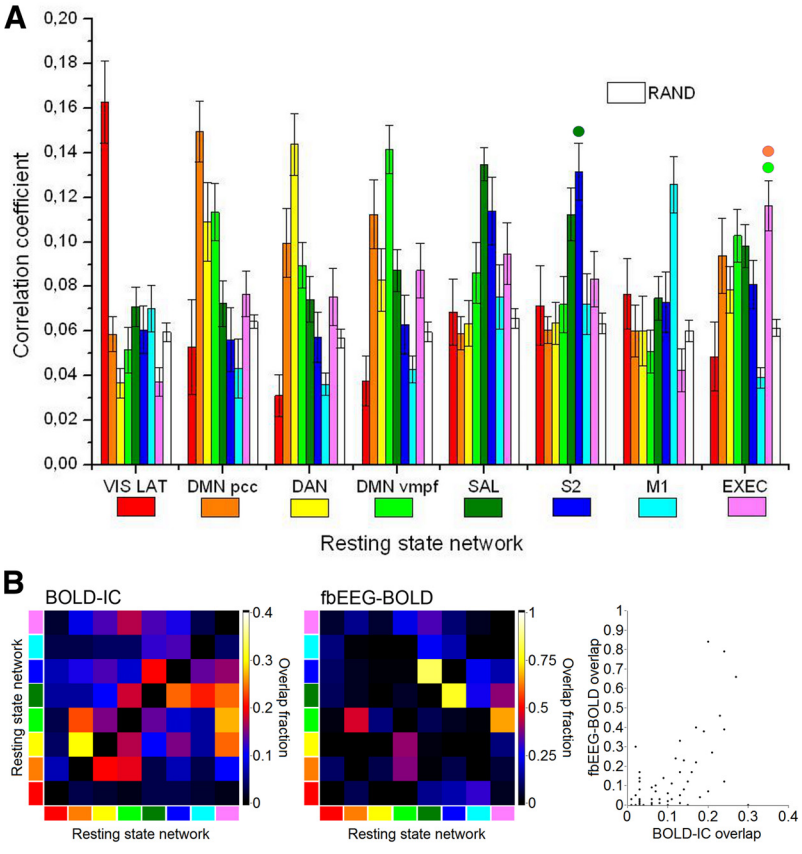

Figure 3. Spatial correlations between fbEEG—fMRIbin maps and BOLD_RSNbin maps are specific to the corresponding BOLD IC for most RSNs and greater than in randomized data. ***A***, Mean correlation coefficients between fbEEG–fMRIbin maps and BOLD_RSNbin maps (error bars indicate SEM). In paired statistical comparisons, for each network between the correlation value for the best-fitting map compared with the other seven, all other differences are significant at $p < 0.05$ (Holm–Bonferroni corrected) except for DMNvmpf-EXEC, DMNpcc-EXEC, and SAL-S2 (marked with colored circles). Maps are organized in descending order of averaged correlation coefficients. ***B***, Spatial overlap between BOLD_RSNbin (left) and fbEEG-fMRIbin (middle) maps was quantified with a correlation coefficient.

data confirmed that at the group level, resting-state fbEEG ICs and fMRI BOLD signals are indeed temporally correlated. Moreover, these data indicate that the correlation between fbEEG ICs and BOLD time series is observed exclusively in anatomically well delineated regions that match those of fMRI ICs remarkably well. To exclude the possibility that the selection criterion could have biased the outcome, we repeated these analyses on randomized DMNpcc fbEEG–fMRIbin maps (Fig. 2, far right column) and found that the observed patterns could not be attributed to random effects or the selection procedure.

To further corroborate these results, we quantified the spatial correlations of the fbEEG versus BOLD maps with each of the eight fMRI RSNs (Fig. 3*A*) and the surrogate data. This analysis showed that for most RSNs, the spatial correlations were specific to the corresponding BOLD IC and much greater than those expected by chance (Fig. 3, RAND bars). While the visual and motor networks were the most isolated correlates of EEG ISFs, the posterior and anterior parts of the DMN (DMNpcc and DMNvmpf, respectively) as well as the salience and S2 networks exhibited clear cross-correlations. These effects are likely to be attributable to positive (DMNpcc and DMNvmpf) or negative (DMN and DAN) time-series correlations among the source regions or to their spatial proximity (SAL and S2), which, because of EEG volume conduction, leads to signal mix-

ing. To address this issue, we quantified separately the spatial overlap of BOLD IC RSNs and EEG_IC versus BOLD maps (Fig. 3*B*). BOLD ICs for S2, SAL, EXEC, and DMNvmpf overlapped with fractions of overlapping area of up to 0.3. Together with the mixing of signals from anatomically nearby sources, this spatial overlap may be reflected in the separability of fbEEG IC versus BOLD maps as well. Indeed, in the maps of fbEEG–BOLD correlation, the overlap was even more pronounced than for BOLD ICs and reached values up to 0.9 for S2–SAL correlation. Importantly, the fbEEG–BOLD map overlaps were strongly correlated with those of BOLD ICs (Pearson $r = 0.59$; $p < 0.000002$; Fig. 3*B*, right), which shows that, despite volume conduction, the fbEEG–BOLD maps capture well the neurophysiological interactions reflected in BOLD–IC RSNs.

Discussion

At the phenomenological level, three kinds of neuronal ISFs characterize spontaneous brain activity and may contribute to slow behavioral dynamics: amplitude and firing rate variability; slow scalp and cortical potentials; and BOLD signal fluctuations (Palva and Palva, 2012). While many correlations among these phenomena have been established, such as the correlation of oscillation amplitude fluctuations with both BOLD signals and slow scalp potentials, direct evidence for a correlation between the spontaneous fluctuations in slow scalp potentials and BOLD signals has not been obtained so far, and the strength of the indirect correlations is insufficient for inferring their association. We performed simultaneous resting-state fbEEG-fMRI recordings, and report here that infra-slow scalp potentials and BOLD signals are correlated. Using ICA, we found that in individual subjects the fbEEG ICs were robustly correlated with subsets of BOLD voxel signals. Both at the single-subject and group levels, the anatomical patterns of fbEEG IC versus BOLD voxel correlations closely matched those of predominant BOLD ICs (Figs. 1, 2). Spontaneous slow potentials in resting-state scalp EEG (Aladjalova, 1964; Trimmel et al., 1990; Marshall et al., 1998; Vanhatalo et al., 2004; Monto et al., 2008) are thus a mixture of superimposed signals pertaining to neuronal activity in anatomically and dynamically distinct RSNs. Hence, the implications of this finding extend much beyond our original hypothesis of a correlation between scalp potential and BOLD ISFs—the anatomical specificity of fbEEG–BOLD correlations with the canonical BOLD RSNs strongly suggests that these phenomena are reflections of shared underlying neuronal and hemodynamic processes.

The relationship among EEG ISFs, slow cortical potentials, and BOLD signal

Around the time of the discovery of spontaneous ISFs in cortical and scalp potentials (Aladjalova, 1957, 1964; Norton and Jewett, 1965), event-related slow potentials also were observed in EEG data averaged across many sensory stimuli or motor actions (Walter et al., 1964; Kornhuber and Deecke, 1965). Cues preceding to-be-attended stimuli are followed by a slow potential shift, "contingent negative variation," of which the magnitude is dependent on the level of expectation toward the forthcoming stimulus (Walter et al., 1964; Gonzalez-Rosa et al., 2011; Werner et al., 2011; Zanto et al., 2011). On the other hand, voluntary movement initiation is preceded by a slow negative "readiness potential" that precedes the movement onset by several hundreds of milliseconds (Kornhuber and Deecke, 1965; Libet et al., 1983; Libet, 1985). Similar sustained slow cortical potentials (SCPs) are also associated with stimuli or experimental manipulations that involve a maintained high level of fast neuronal activity. For instance, these SCPs are correlated with attentional memory (Hansen and Hillyard, 1980; Luria and Vogel, 2011), working memory (Vogel and Machizawa, 2004; Vogel et al., 2005; McCollough et al., 2007; Palva et al., 2011), and long-term memory (Khader et al., 2007; Kizilirmak et al., 2012) demands as well as with mental imagery (Schicke et al., 2006). Similarly, intense neuronal activity during epileptic seizures is associated with sustained negative shifts in scalp potentials (Vanhatalo et al., 2003a).

Several lines of research indicate a correlation between event-related SCPs and BOLD signals (Leistner et al., 2007, 2010; Khader et al., 2008; see Introduction), and also provide indirect evidence for a similar relationship between spontaneous SCPs and BOLD signals (He et al., 2008; Helps et al., 2010; Broyd et al., 2011). Such observations constitute the basis for a hypothesis that SCPs are a direct electrophysiological correlate of BOLD signals (He et al., 2008; He and Raichle, 2009; Raichle, 2011). If spontaneous EEG ISFs are considered as SCPs (Rockstroh et al., 1989; Raichle, 2011), the present results both corroborate this idea and extend the prior data in showing with simultaneous fbEEG and fMRI that spontaneous SCPs are indeed correlated with BOLD signals and that these correlations are specific to well delineated RSNs.

It has, however, remained unresolved whether a universal SCP–BOLD correlation exists that spans both event-related and spontaneous SCPs. First, the relationship between event-related SCPs and spontaneous fluctuations has remained unclear and, to our knowledge, there is no evidence that the event-related SCPs would arise from event-locking of spontaneous SCPs (but see Raichle, 2011). Second, slow phenomena span a wide range of time scales (Rockstroh et al., 1989). Perievent SCPs last from hundreds of milliseconds to a few seconds and hence reside in slow-frequency (0.1–1 Hz) and delta-frequency (1–4 Hz) bands. Spontaneous potential and BOLD ISFs also involve time scales from tens to hundreds of seconds. Third, there could be differences in the underlying neuronal generators. Event-related SCPs appear to arise in task-specific circuitry, while the spontaneous ISFs are well correlated with RSNs, in which the interaction with task-specific processing is not fully understood. Spontaneous ISFs, on the other hand, appear to be supported by oscillatory and time scale-specific cellular-level mechanisms (Lörincz et al., 2009; Hughes et al., 2011). Hence, the relationship between spontaneous and event-related slow potentials remains an important topic for future research and could be addressed both with fbEEG-near-infrared spectroscopy (Leistner et al., 2007, 2010) and, as done here, with fbEEG-fMRI approaches.

Mechanisms linking fbEEG and BOLD ISF signals

Several lines of evidence, including concurrent recordings of scalp potentials, intracortical field potentials, and neuronal membrane potentials, suggest that slow negative shifts in scalp EEG arise from synaptic excitation of the apical dendrites of cortical pyramidal neurons (Mitzdorf, 1985; Birbaumer et al., 1990; He and Raichle, 2009). In this context, enhanced cortical excitability and possibly intense neuronal activity would be associated in parallel with long-lasting excitatory postsynaptic potentials, negative scalp potentials, and enhanced BOLD signal. Spontaneous fluctuations in neuronal activity levels could hence be reflected in parallel both in slow potentials and hemodynamic signals.

Slow cortical and scalp potentials may, however, also involve non-neuronal mechanisms, and in particular, a direct contribution from the potential difference across the blood–brain barrier, which is sensitive to many manipulations of hemodynamics and

brain carbon dioxide levels (Besson et al., 1970; Vanhatalo et al., 2003b; Voipio et al., 2003; Nita et al., 2004). It is thus possible that the endogenous BOLD fluctuations per se directly contribute to the observations of spontaneous slow scalp potentials such as those observed here and earlier.

Conclusion

In the present study, we show that spontaneous infra-slow scalp potential fluctuations are correlated with endogenous BOLD signal fluctuations in brain regions corresponding to canonical fMRI RSNs.

References

Aladjalova NA (1957) Infra-slow rhythmic oscillations of the steady potential of the cerebral cortex. Nature 179:957–959. CrossRef Medline

Aladjalova NA (1964) Infraslow potential oscillations in the cerebral cortex. In: Progress in brain research: slow electrical processes in the brain, Vol 7 (Aladjalova NA, ed), pp 39–58. New York: Elsevier.

Albrecht D, Gabriel S (1994) Very slow oscillations of activity in geniculate neurones of urethane-anaesthetized rats. Neuroreport 5:1909–1912. CrossRef Medline

Allen PJ, Polizzi G, Krakow K, Fish DR, Lemieux L (1998) Identification of EEG events in the MR scanner: the problem of pulse artifact and a method for its subtraction. Neuroimage 8:229–239. CrossRef Medline

Allen PJ, Josephs O, Turner R (2000) A method for removing imaging artifact from continuous EEG recorded during functional MRI. Neuroimage 12:230–239. CrossRef Medline

Allers KA, Ruskin DN, Bergstrom DA, Freeman LE, Ghazi LJ, Tierney PL, Walters JR (2002) Multisecond periodicities in basal ganglia firing rates correlate with theta bursts in transcortical and hippocampal EEG. J Neurophysiol 87:1118–1122. Medline

Beckmann CF, Smith SM (2004) Probabilistic independent component analysis for functional magnetic resonance imaging. IEEE Trans Med Imaging 23:137–152. CrossRef Medline

Bell AJ, Sejnowski TJ (1995) An information-maximization approach to blind separation and blind deconvolution. Neural Comput 7:1129–1159. CrossRef Medline

Besson JM, Woody CD, Aleonard P, Thompson HK, Albe-Fessard D, Marshall WH (1970) Correlations of brain d-c shifts with changes in cerebral blood flow. Am J Physiol 218:284–291. Medline

Birbaumer N, Elbert T, Canavan AG, Rockstroh B (1990) Slow potentials of the cerebral cortex and behavior. Physiol Rev 70:1–41. Medline

Biswal B, Yetkin FZ, Haughton VM, Hyde JS (1995) Functional connectivity in the motor cortex of resting human brain using echo-planar MRI. Magn Reson Med 34:537–541. CrossRef Medline

Broyd SJ, Helps SK, Sonuga-Barke EJ (2011) Attention-induced deactivations in very low frequency EEG oscillations: differential localisation according to ADHD symptom status. PLoS One 6:e17325. CrossRef Medline

Damoiseaux JS, Rombouts SA, Barkhof F, Scheltens P, Stam CJ, Smith SM, Beckmann CF (2006) Consistent resting-state networks across healthy subjects. Proc Natl Acad Sci U S A 103:13848–13853. CrossRef Medline

Delorme A, Makeig S (2004) EEGLAB: an open source toolbox for analysis of single-trial EEG dynamics including independent component analysis. J Neurosci Methods 134:9–21. CrossRef Medline

De Luca M, Beckmann CF, De Stefano N, Matthews PM, Smith SM (2006) fMRI resting state networks define distinct modes of long-distance interactions in the human brain. Neuroimage 29:1359–1367. CrossRef Medline

Fox MD, Snyder AZ, Vincent JL, Corbetta M, Van Essen DC, Raichle ME (2005) The human brain is intrinsically organized into dynamic, anticorrelated functional networks. Proc Natl Acad Sci U S A 102:9673–9678. CrossRef Medline

Goldman RI, Stern JM, Engel J Jr, Cohen MS (2002) Simultaneous EEG and fMRI of the alpha rhythm. Neuroreport 13:2487–2492. CrossRef Medline

Gonzalez-Rosa JJ, Vazquez-Marrufo M, Vaquero E, Duque P, Borges M, Gomez-Gonzalez CM, Izquierdo G (2011) Cluster analysis of behavioural and event-related potentials during a contingent negative variation paradigm in remitting-relapsing and benign forms of multiple sclerosis. BMC Neurol 11:64. CrossRef Medline

Hansen JC, Hillyard SA (1980) Endogenous brain potentials associated with selective auditory attention. Electroencephalogr Clin Neurophysiol 49:277–290. Medline

He BJ, Raichle ME (2009) The fMRI signal, slow cortical potential and consciousness. Trends Cogn Sci 13:302–309. CrossRef Medline

He BJ, Snyder AZ, Zempel JM, Smyth MD, Raichle ME (2008) Electrophysiological correlates of the brain's intrinsic large-scale functional architecture. Proc Natl Acad Sci U S A 105:16039–16044. CrossRef Medline

Helps SK, Broyd SJ, James CJ, Karl A, Chen W, Sonuga-Barke EJ (2010) Altered spontaneous low frequency brain activity in attention deficit/hyperactivity disorder. Brain Res 1322:134–143. CrossRef Medline

Hughes SW, Lorincz ML, Parri HR, Crunelli V (2011) Infraslow (<0.1 hz) oscillations in thalamic relay nuclei basic mechanisms and significance to health and disease states. Prog Brain Res 193:145–162. CrossRef Medline

Jenkinson M, Bannister P, Brady M, Smith S (2002) Improved optimization for the robust and accurate linear registration and motion correction of brain images. Neuroimage 17:825–841. CrossRef Medline

Khader P, Knoth K, Burke M, Ranganath C, Bien S, Rosler F (2007) Topography and dynamics of associative long-term memory retrieval in humans. J Cogn Neurosci 19:493–512. CrossRef Medline

Khader P, Schicke T, Röder B, Rösler F (2008) On the relationship between slow cortical potentials and BOLD signal changes in humans. Int J Psychophysiol 67:252–261. CrossRef Medline

Kizilirmak JM, Rosler F, Khader PH (2012) Control processes during selective long-term memory retrieval. Neuroimage 59:1830–1841. CrossRef Medline

Ko AL, Darvas F, Poliakov A, Ojemann J, Sorensen LB (2011) Quasi-periodic fluctuations in default mode network electrophysiology. J Neurosci 31:11728–11732. CrossRef Medline

Kornhuber HH, Deecke L (1965) Changes in the brain potential in voluntary movements and passive movements in man: readiness potential and reafferent potentials. Pflugers Arch Gesamte Physiol Menschen Tiere 284:1–17. CrossRef Medline

Leistner S, Sander T, Burghoff M, Curio G, Trahms L, Mackert BM (2007) Combined MEG and EEG methodology for non-invasive recording of infraslow activity in the human cortex. Clin Neurophysiol 118:2774–2780. CrossRef Medline

Leistner S, Sander TH, Wuebbeler G, Link A, Elster C, Curio G, Trahms L, Mackert BM (2010) Magnetoencephalography discriminates modality-specific infraslow signals less than 0.1 hz. Neuroreport 21:196–200. CrossRef Medline

Leopold DA, Murayama Y, Logothetis NK (2003) Very slow activity fluctuations in monkey visual cortex: implications for functional brain imaging. Cereb Cortex 13:422–433. CrossRef Medline

Libet B (1985) Unconscious cerebral initiative and the role of conscious will in voluntary action. Behav Brain Sci 8:5259–5566.

Libet B, Gleason CA, Wright EW, Pearl DK (1983) Time of conscious intention to act in relation to onset of cerebral activity (readiness-potential). the unconscious initiation of a freely voluntary act. Brain 106:623–642. Medline

Linkenkaer-Hansen K, Nikouline VV, Palva JM, Ilmoniemi RJ (2001) Long-range temporal correlations and scaling behavior in human brain oscillations. J Neurosci 21:1370–1377. Medline

Lörincz ML, Geall F, Bao Y, Crunelli V, Hughes SW (2009) ATP-dependent infra-slow (<0.1 hz) oscillations in thalamic networks. PLoS One 4:e4447. CrossRef Medline

Lowe MJ, Mock BJ, Sorenson JA (1998) Functional connectivity in single and multislice echoplanar imaging using resting-state fluctuations. Neuroimage 7:119–132. CrossRef Medline

Luria R, Vogel EK (2011) Visual search demands dictate reliance on working memory storage. J Neurosci 31:6199–6207. CrossRef Medline

Mantini D, Perrucci MG, Del Gratta C, Romani GL, Corbetta M (2007) Electrophysiological signatures of resting state networks in the human brain. Proc Natl Acad Sci U S A 104:13170–13175. CrossRef Medline

Marshall L, Mölle M, Fehm HL, Born J (1998) Scalp recorded direct current brain potentials during human sleep. Eur J Neurosci 10:1167–1178. CrossRef Medline

McCollough AW, Machizawa MG, Vogel EK (2007) Electrophysiological measures of maintaining representations in visual working memory. Cortex 43:77–94. Medline

Mitzdorf U (1985) Current source-density method and application in cat cerebral cortex: investigation of evoked potentials and EEG phenomena. Physiol Rev 65:37–100. Medline

Monto S, Vanhatalo S, Holmes MD, Palva JM (2007) Epileptogenic neocortical networks are revealed by abnormal temporal dynamics in seizure-free subdural EEG. Cereb Cortex 17:1386–1393. CrossRef Medline

Monto S, Palva S, Voipio J, Palva JM (2008) Very slow EEG fluctuations predict the dynamics of stimulus detection and oscillation amplitudes in humans. J Neurosci 28:8268–8272. CrossRef Medline

Nita DA, Vanhatalo S, Lafortune FD, Voipio J, Kaila K, Amzica F (2004) Nonneuronal origin of CO2-related DC EEG shifts: an in vivo study in the cat. J Neurophysiol 92:1011–1022. CrossRef Medline

Norton S, Jewett RE (1965) Frequencies of slow potential oscillations in the cortex of cats. Electroencephalogr Clin Neurophysiol 19:377–386. CrossRef Medline

Palva S, Kulashekhar S, Hamalainen M, Palva JM (2011) Localization of cortical phase and amplitude dynamics during visual working memory encoding and retention. J Neurosci 31:5013–5025. CrossRef Medline

Palva JM, Palva S (2012) Infra-slow fluctuations in electrophysiological recordings, blood-oxygenation-level-dependent signals, and psychophysical time series. Neuroimage 62:2201–2211. CrossRef Medline

Raichle ME (2011) The restless brain. Brain Connect 1:3–12. CrossRef Medline

Raichle ME, MacLeod AM, Snyder AZ, Powers WJ, Gusnard DA, Shulman GL (2001) A default mode of brain function. Proc Natl Acad Sci U S A 98:676–682. CrossRef Medline

Rockstroh B, Elbert T, Canavan AG, Lutzenberger W, Birbaumer N (1989) Slow cortical potentials and behavior, Ed 2. Baltimore, MD: Urban and Schwarzenberg.

Ruskin DN, Bergstrom DA, Kaneoke Y, Patel BN, Twery MJ, Walters JR (1999) Multisecond oscillations in firing rate in the basal ganglia: robust modulation by dopamine receptor activation and anesthesia. J Neurophysiol 81:2046–2055. Medline

Ruskin DN, Bergstrom DA, Tierney PL, Walters JR (2003) Correlated multisecond oscillations in firing rate in the basal ganglia: modulation by dopamine and the subthalamic nucleus. Neuroscience 117:427–438. CrossRef Medline

Sadaghiani S, Scheeringa R, Lehongre K, Morillon B, Giraud AL, Kleinschmidt A (2010) Intrinsic connectivity networks, alpha oscillations, and tonic alertness: a simultaneous electroencephalography/functional magnetic resonance imaging study. J Neurosci 30:10243–10250. CrossRef Medline

Schicke T, Muckli L, Beer AL, Wibral M, Singer W, Goebel R, Rosler F, Roder B (2006) Tight covariation of BOLD signal changes and slow ERPs in the parietal cortex in a parametric spatial imagery task with haptic acquisition. Eur J Neurosci 23:1910–1918. CrossRef Medline

Seeley WW, Menon V, Schatzberg AF, Keller J, Glover GH, Kenna H, Reiss AL, Greicius MD (2007) Dissociable intrinsic connectivity networks for salience processing and executive control. J Neurosci 27:2349–2356. CrossRef Medline

Smith SM (2002) Fast robust automated brain extraction. Hum Brain Mapp 17:143–155. CrossRef Medline

Trimmel M, Mikowitsch A, Groll-Knapp E, Haider M (1990) Occurrence of infraslow potential oscillations in relation to task, ability to concentrate and intelligence. Int J Psychophysiol 9:167–170. CrossRef Medline

Vanhatalo S, Holmes MD, Tallgren P, Voipio J, Kaila K, Miller JW (2003a) Very slow EEG responses lateralize temporal lobe seizures: an evaluation of non-invasive DC-EEG. Neurology 60:1098–1104. CrossRef Medline

Vanhatalo S, Tallgren P, Becker C, Holmes MD, Miller JW, Kaila K, Voipio J (2003b) Scalp-recorded slow EEG responses generated in response to hemodynamic changes in the human brain. Clin Neurophysiol 114:1744–1754. CrossRef Medline

Vanhatalo S, Palva JM, Holmes MD, Miller JW, Voipio J, Kaila K (2004) Infraslow oscillations modulate excitability and interictal epileptic activity in the human cortex during sleep. Proc Natl Acad Sci U S A 101:5053–5057. CrossRef Medline

Vogel EK, Machizawa MG (2004) Neural activity predicts individual differences in visual working memory capacity. Nature 428:748–751. CrossRef Medline

Vogel EK, McCollough AW, Machizawa MG (2005) Neural measures reveal individual differences in controlling access to working memory. Nature 438:500–503. CrossRef Medline

Voipio J, Tallgren P, Heinonen E, Vanhatalo S, Kaila K (2003) Millivolt-scale DC shifts in the human scalp EEG: evidence for a nonneuronal generator. J Neurophysiol 89:2208–2214. Medline

Walter WG, Cooper R, Aldridge VJ, McCallum WC, Winter AL (1964) Contingent negative variation: an electric sign of sensorimotor association and expectancy in the human brain. Nature 203:380–384. CrossRef Medline

Werner G, Mountcastle VB (1963) The variability of central neural activity in a sensory system, and its implications for the central reflection of sensory events. J Neurophysiol 26:958–977. Medline

Werner J, Weisbrod M, Resch F, Roessner V, Bender S (2011) Increased performance uncertainty in children with ADHD? Elevated post-imperative negative variation (PINV) over the ventrolateral prefrontal cortex. Behav Brain Funct 7:38. CrossRef Medline

Zanto TP, Pan P, Liu H, Bollinger J, Nobre AC, Gazzaley A (2011) Age-related changes in orienting attention in time. J Neurosci 31:12461–12470. CrossRef Medline